Control of a Wind Farm Connected to the Grid at a Frequency and Variable Voltage

Youssef Krim‡*, Saber Krim*, Mohamed Faouzi Mimouni*

*National Engineering School of Monastir, Electrical Engineering Department, 5019 Monastir–Tunisia

(Krim_enim@hotmail.com, krimsaber@hotmail.fr, Mfaouzi.mimoni@enim.rnu.tn)

‡ Youssef KRIM; Address: National Engineering School of Monastir, Research Unit "Industrial Systems Study and Renewable Energy", 5019 Monastir – Tunisia, Tel: (+216) 73 500 511, Fax: (+216) 73 500 514

Received: 24.02.2016 Accepted:30.06.2016

Abstract - Wind energy is characterized by fluctuation because of a main intermittent source, which can damage the stability of the electrical network which leads to an imbalance between production and consumption. To resolve this difficulty, an integration of a micro-grid based on a wind farm interconnected to the electricity grid is proposed which presents the first objective of this paper. The two-level inverter is so much used in this domain, but the main limitations of this solutions are the fact that the voltage output presents high ripples and that this inverter is not a practical solution for applications with high power. Thus, the second aim of this paper consists in using a multicellular inverter. The main unit of this farm is based on a three permanent magnet synchronous generators which are entrained by three aero-generators. This unity is connected to a DC bus through three controlled rectifiers. The obtained power is injected to the electricity grid using a multicellular inverter as well as an inductor and resistor filter. The three generators and the proposed inverter are controlled through a vector control. A theoretical study of the suggested farm is parented and simulated using a Matlab/Simulink environment. The obtained simulation results confirm the approach robustness.

Keywords- Wind farm, PMSG, Multicellular Converters, Micro-Grid (MG), Pitch angle.

1. Introduction

The consumption of electricity has increased dramatically over the past decade because of the massive industrialization of some countries and the significant population increase. During the first half of the century, fossil fuels remain the main source of energy, which consequently causes environmental problems in terms of global warming and climate change. All these reasons have contributed to the growing penetration of renewable energy to generate the electricity [1]. The use of this type of energy has several advantages [2], like reducing one greenhouse gas emissions, improving the voltage profile and ensuring the quality of energy. The most common way to add renewable energy systems to the grid is the Micro-Grid (MG). The MG is considered as a grid that contains fillers and generators [3, 4] used to facilitate the strong penetration of renewable generators, like wind, solar and geothermal energies. These renewable generators reduce the consumption of fossil fuel and CO_2 emissions [5].

In this general context, this paper focuses on the wind power. It is characterized by a growth rate of Use high compared to other types of renewable energy. Nowadays, wind energy is evolving in a rapid and massive way. This evolution is described by the increase in installed capacity worldwide [6, 7]. The major drawback of this type of production is the unsteady state of its primary source (the wind) [8]. This makes the wind generator unable to contribute in system services, namely voltage control, control of reactive power and the frequency setting. To solve this problem, related to limiting the penetration of wind generators into the electricity grid, several approaches have added energy storage devices [9, 10, 11]. In this paper, this problem is developed by concentrating on the integration of a micro-grid based on a wind farm to the electricity network. This farmhouse is made by the association of three wind generators based on a Permanent Magnet Synchronous Generator (PMSG).

Increasing levels of the voltage modulated by the converter is used to reduce the harmonic distortion of this

voltage. The concept of a multilevel voltage inverter has been introduced to decrease the harmonic distortion of output waves, without reducing the output power converters [12].

In this paper, our study focuses on a multi-inverter instead of a two-level inverter, thanks to its many advantages. In recent years, the uses of multicellular inverters in industrial applications have risen [13, 14]. A multicellular inverter is formed by switches and capacitors as voltage sources [15]. This type of inverter is used for high power applications. In this study, a four-cell inverter is utilized to illustrate this trade off. Therefore, it is a five-level inverter.

The first part of our study focuses on modeling of the various parts of the production unit. In the second part, we presented the different control techniques applied two vector commands of the generators 2 and 3 to insure the monitoring of the Maximum Power Point tracking (MPPT) and a vector control of the generator 1 has been implemented for the adjustment of the DC bus voltage. Finally, a vector control of the inverter was developed based on the management of power injected into the grid. The simulation results allow validating the implemented control strategies.

2. Modeling of the Wind Farm

The system studied is shown by Fig.1. This farm consists of three aero-generators, where each one is connected to a variable speed synchronous generator. For operation at variable speed, three rectifiers are used to connect the generators to the DC bus. This bus is linked to the electrical network via multilevel inverter and an RL (resistance R and inductor L) filter.

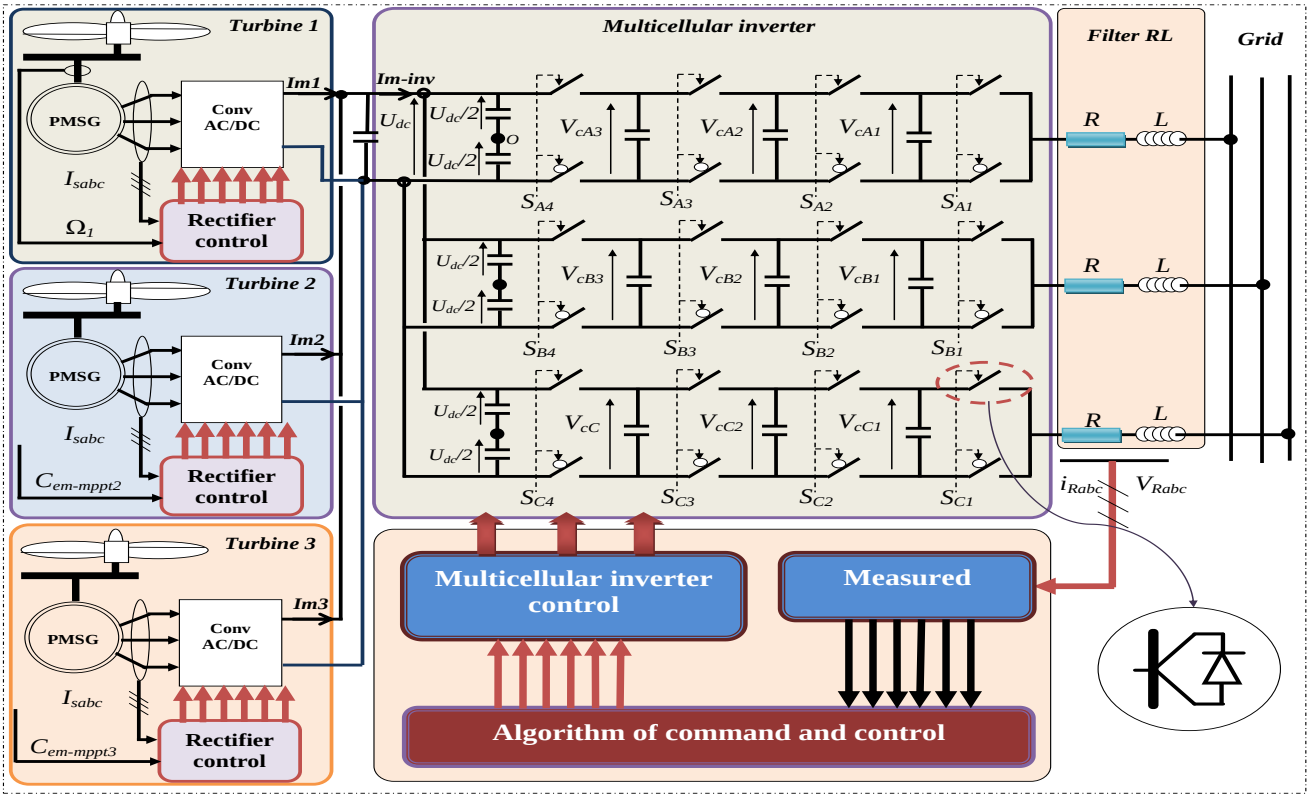

Fig 1. Architecture of proposed wind farm

2.1. Wind turbine modeling and control

The wind power produced by each turbine is given by the following expression [16]:

$$P_{aer} = C_p.P_w = \frac{1}{2}.C_p.\rho.S.V_v^3 \quad (1)$$

where ρ is the density of the air (kg/m3), S is the area swept by the turbine (m2), V_v is the speed of wind (m/s) and $C_p(\lambda,\beta)$ (power coefficient) depends on the pitch angle β and of the specific speed λ. This coefficient described by the equation (2) and (3) [17]:

$$C_p = 0.5872.(116.\lambda_i - 0.4*\beta - 5).e^{-21.\lambda_i} + 0.0085.\lambda \quad (2)$$

with

$$\lambda_i = \frac{1}{\lambda + 0.008\beta} - \frac{0.035}{\beta + 1} \quad (3)$$

where λ is defined by the ratio between the turbine rotation speed and wind speed:

$$\lambda = \frac{R.\Omega_{turbine}}{V_v} \quad (4)$$

Knowing the speed of the turbine, the aerodynamic torque is determined by:

$$C_{aer} = \frac{P_{aer}}{\Omega_{turbine}} = C_p . \frac{P_v}{\Omega_{turbine}} = C_p . \frac{\rho.S.V^3}{2.\Omega_{turbine}} \quad (5)$$

The fundamental equation of the dynamic enables determining the evolution of the rotation speed of the generator Ωmec.

$$J . \frac{d\Omega_{mec}}{dt} = C_{aer} - C_{em} - C_{vis} \quad (6)$$

where C_{vis} is the viscous friction torque and C_{em} is the electromagnetic torque.

The wind farm is controlled to extract the maximum power available. According to the Betz theory, the power coefficients Cp do not exceed 0.593 [18, 19], which correspond to the Betz limit. Therefore, the power produced by a turbine is 59.3% of the available power of wind.

In this case, the variation of *Cp* as a function of λ for β = 0 is shown in Fig.2, then the maximum value of *Cp* (C_{pmax}=0.55) is corresponding to the optimal value of λ (λ_{opt}=8.1).

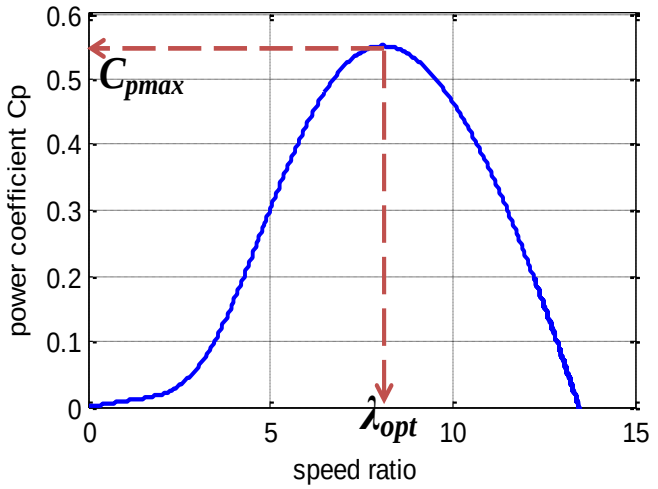

Fig. 2. Cp versus λ curve

The electromagnetic torque reference given by the MPPT strategy is defined by Equation (7) [18, 19].

$$C_{em-MPPT} = \frac{C_p . \rho . \pi . R^5 . \Omega^2_{mec}}{2 . \lambda^3_{opt} . G^3} \quad (7)$$

2.2. Control of the pitch angle

In order to reduce speed and avoid mechanical faults, a blade guidance system is needed to serve as a regulator. In this context, to ensure the safety of the machine used for the wind generator, it is necessary to limit its speed. This limitation is made by the setting angle of the blades β. When the speed exceeds its nominal value Ω_{mecn}, the power coefficient C_p decreases by increasing the angle β. This control strategy is described by the following equations:

$$\begin{cases} \beta_{ref} = \beta_0 = 0 \ \ for \ 0 \le \Omega_{mec} \le \Omega_{mecn} \\ \beta_{ref} = \dfrac{\Delta\beta}{\Delta\Omega_{mec}} (\Omega_{mec} - \Omega_{mecn}) \ for \ \Omega_{mec} \ge \Omega_{mecn} \end{cases} \quad (8)$$

where β_0 is the initial pitch angle.

In most cases, the blade guidance system can be electrical or hydraulic. We can thus introduce a transfer function of the first order to simulate the dynamics of the angle β according to the next reference [20, 21].

$$\beta = \frac{1}{1 + \tau_b . S} . \beta_{ref} \quad (9)$$

where τ_b is the time constant of the blades' orientation system and S is the Laplace operator.

Figure 3 shows the block diagram of the turbine with the guidance system of the blades:

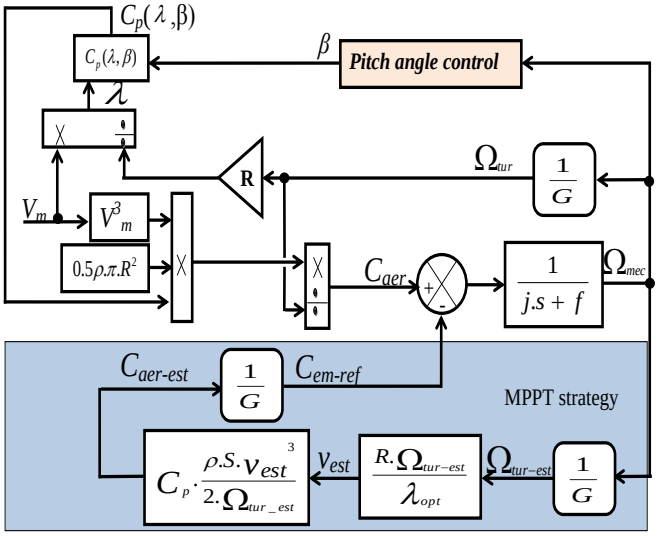

Fig.3. Turbine model with pitch control method

2.3. Modeling and control of PMSG

The permanent magnet machines are increasingly used in the field of electricity production.

The equations utilized for modeling the PMSG in the park reference frame under the MATLAB/Simulink tool are [22]:

$$\begin{cases} V_{sd} = V_{sd1} - p.\Omega.L_s.i_{sq} \\ V_{sq} = V_{sq1} + p.\Omega.L_s.i_{sd} + p\Omega\phi \end{cases} \quad (10)$$

$$\begin{cases} V_{sd1} = L_s \dfrac{di_{sd}}{dt} + R_s.i_{sd} \\ V_{sq1} = L_s \dfrac{di_{sq}}{dt} + R_s.i_{sq} \end{cases} \quad (11)$$

The electromagnetic torque is given by:

$$C_{em} = p.\phi_m.i_{sq} \quad (12)$$

where R_s is the resistance of each stator winding (Ω), L_s is the inductance of each stator winding (H), Φ_m is the flux induced by the permanent magnets (wb), i_{sd} and i_{sq} are the direct and quadratic component of the stator current, V_{sd} and V_{sq} are the direct and quadratic component of the stator voltage, and p is the pole pair number.

The principle of this control is to divide the farm into two groups. The first group contains turbines 2 and 3. They only work in the MPPT to participate in the system service. This command allows imposing a direct current reference i_{sd} equal to zero to minimize resistive losses. The electromagnetic torque depends only on the stator current i_{sq}. Since the flux is constant, so the torque and the current i_{sq} are proportional.

$$i^*_{sq} = \frac{C_{em-mppt}}{p.\phi_m} \tag{13}$$

with $C_{em-mppt}$ is given by equation (7).

The second group contains turbine 1, but this turbine does not work in the MPPT. It is also responsible for regulating the DC bus voltage. This command requires a direct current reference equal to zero to minimize resistive losses and the DC bus voltage is controlled by the stator current i_{sq}:

$$i^*_{sq} = \frac{C^*_{em}}{p.\phi_m} \tag{14}$$

with:

$$C^*_{em} = \frac{P_{g1}}{\Omega_1} = \frac{U_{bus}.i_{m1}}{\Omega_1} \tag{15}$$

The block diagram of the control loops of the stator currents is given by the following figure:

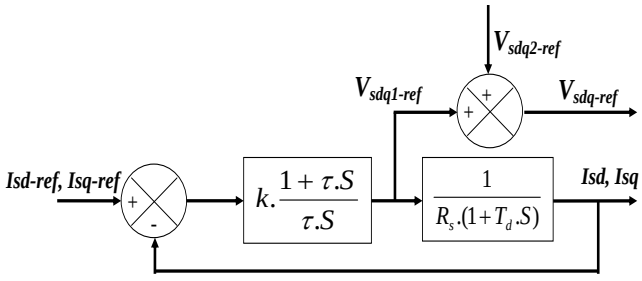

Fig. 4. Control system of stator currents

with:

$K = 3.\frac{L_s}{t_r}$: the gain of the controller

t_r: the response time

$T_d = \tau = \frac{L_s}{R_s}$: the coefficient of the integral controller.

R_s: the stator resistance (Ω)

L_s: the stator inductance (H)

2.4. DC bus modeling and control

The DC bus voltage U_{dc} changes according to the following equation:

$$\frac{dU_{bus}}{dt} = \frac{1}{C} i_{bus} = \frac{1}{C}.(\sum_{i=1}^{3} i_{mi} - i_{m-inv}) \tag{16}$$

where i_{mi}: is current modulated by each PMSG and $i_{m-inv} = \frac{1}{2}(U_{rdw}.i_d + U_{rqw}.i_q)$ is the current modulated by the inverter.

The proportional integral regulator (PI) is applied to keep the measured voltage U_{bus} equivalent to the $U_{bus-ref}$ reference. The control loops are adapted diagrammatically in Fig.5:

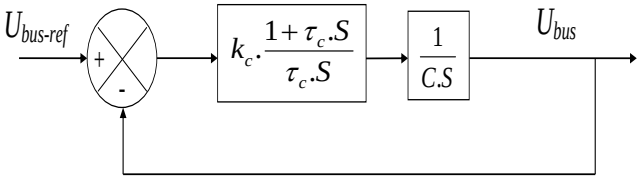

Fig. 5. DC bus control loop

with:

$$\tau_c = \frac{2.\xi.t_r}{3} \tag{17}$$

$$k_c = \frac{6.C.\xi}{t_c} \tag{18}$$

2.5. Rectifier modeling

The studied AC / DC converter is composed of three arms. Each one is composed of two IGBTs. It is connected to the generator and operates as a controlled rectifier. The switches of the same arm are controlled in a complementary manner to avoid the short circuit of the voltage source. Then, we have:

$$f_{1i} + f_{2i} = 1 \quad \text{With } i \in \{1,2,3\}$$

The expressions of direct and quadratic voltages V_{sd} and V_{sq}, modulated by the converter depend on the direct and quadratic control voltages, U_{sdw} and U_{sqw}, of the converter.

$$\begin{pmatrix} V_{sd} \\ V_{sq} \end{pmatrix} = \frac{U_{bus}}{2} \begin{pmatrix} U_{sdw} \\ U_{sqw} \end{pmatrix} \tag{19}$$

The current modulated by the converter can be calculated by this expression:

$$i_{mi} = \frac{1}{2}.(U_{sdwi}.i_{sdi} + U_{sqwi}.i_{sqi}), i \in \{1,2,3\} \tag{20}$$

Finally, the generator side control strategy applied to our wind farm is given by the following figure:

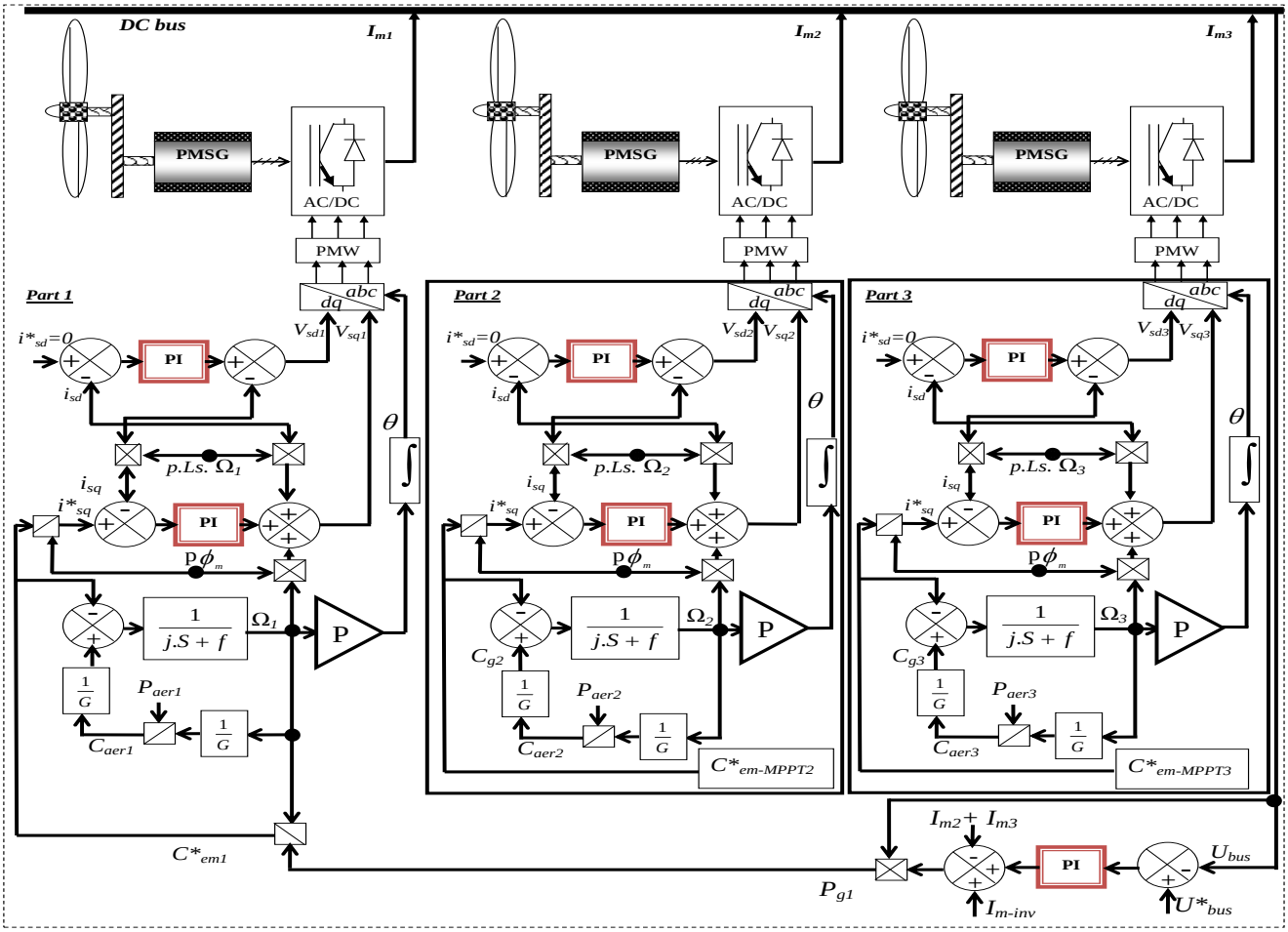

Fig. 6. Proposed control strategy applied to our wind farm

3. Control of Powers Injected to the AC Grid

The power supplied by the PMSGs is applied to an inverter through a DC bus. This inverter permits to controlling the reactive and active power injected to the electrical network characterized by a frequency f = 50 Hz and voltage V_R.

This study focuses on a multicellular inverter. This inverter consists of *K* cells. Each cell is composed of two switches and two capacitors as voltage sources. The switches operate in a complementary manner.

In this paper, we have studied a four-cell converter. Fig. 1 shows the internal structure of the studied converter.

3.1. Modeling multicellular converter

The voltages across the floating capacitors V_{cij} vary depending on the current I_{Ri}.

where *i* (i=A, B, C) denotes the phase, *j* (*j*=1, 2, 3, 4) designates the concerned cell, and I_{Ri} is the current modulated by the inverter and injected into the grid.

To a multicellular inverter, the current flowing through the floating capacitor is expressed as a function of control signals of the switches next to the capacitor [23]:

$$i_{cij} = (S_{i(j+1)} - S_{ij}) i_{Ri} \tag{21}$$

On the other hand, the current is expressed by:

$$i_{cij} = C_{ij} \cdot \frac{d}{dt} . V_{cij} \tag{22}$$

Then we know the value of the capacitor C_{ij}, so we can get the equation governing the evolution of the V_{cij} tension:

$$\frac{d}{dt} V_{cij} = \frac{1}{C_{ij}} (S_{i(j+1)} - S_{ij}) i_{Ri} \tag{23}$$

Our inverter has three arms, where each consists of four cells (5 levels). The voltages of the capacitors of each arm are expressed as follows:

For arm A:

$$\begin{cases} \frac{d}{dt} V_{cA1} = \frac{1}{C_{A1}} (S_{A2} - S_{A1}) i_{RA} \\ \frac{d}{dt} V_{cA2} = \frac{1}{C_{A2}} (S_{A3} - S_{A2}) i_{RA} \\ \frac{d}{dt} V_{cA3} = \frac{1}{C_{A3}} (S_{A4} - S_{A3}) i_{RA} \end{cases} \tag{24}$$

For arm B:

$$\begin{cases} \frac{d}{dt}V_{cB1} = \frac{1}{C_{B1}}(S_{B2} - S_{B1})i_{RB} \\ \frac{d}{dt}V_{cB2} = \frac{1}{C_{B2}}(S_{B3} - S_{B2})i_{RB} \\ \frac{d}{dt}V_{cB3} = \frac{1}{C_{B3}}(S_{B4} - S_{B3})i_{RB} \end{cases} \quad (25)$$

For arm C:

$$\begin{cases} \frac{d}{dt}V_{cC1} = \frac{1}{C_{C1}}(S_{C2} - S_{C1})i_{RC} \\ \frac{d}{dt}V_{cC2} = \frac{1}{C_{C2}}(S_{C3} - S_{C2})i_{RC} \\ \frac{d}{dt}V_{cC3} = \frac{1}{C_{C3}}(S_{C4} - S_{C3}3)i_{RC} \end{cases} \quad (26)$$

The output voltage V_s corresponds to the sum of the voltages of the terminals of the switches.

These voltages are defined by:

$$V_{\bar{S}ij} = S_{ij}.(V_{cij} - V_{Ci(j-1)}) \quad (27)$$

This implies that the expression of the voltage Vs is written as follows:

$$V_{Si} = \sum_{j=1}^{K} V_{\bar{S}ij} = \sum_{j=1}^{K} S_{ij}.(V_{cij} - V_{ci(j-1)}) \quad (28)$$

From here we can write:

$$V_{S1} = \frac{U_{bus}}{K}.\sum_{j=1}^{K} S_{ij} \quad (29)$$

The voltage across the load is then:

$$V_{chi} = V_{Sj} - \frac{U_{bus}}{2} = R_i.i_i + L_i.\frac{di_i}{dt} \quad (30)$$

The output voltages of the inverter against the fictitious point O are given by:

For arm A:

$$V_{AO} = (S_{A1} - S_{A2}).V_{CA1} + (S_{A2} - S_{A3}).V_{CA2} + (S_{A3} - S_{A4}).V_{CA3} + S_{A4}U_{bus} \quad (31)$$

For arm B:

$$V_{BO} = (S_{B1} - S_{B2}).V_{CB1} + (S_{B2} - S_{B3}).V_{CB2} + (S_{B3} - S_{B4}).V_{CB3} + S_{B4}U_{bus} \quad (32)$$

For arm C:

$$V_{CO} = (S_{C1} - S_{C2}).V_{CC1} + (S_{C2} - S_{C3}).V_{CC2} + (S_{C3} - S_{C4}).V_{CC3} + S_{C4}U_{bus} \quad (33)$$

Then the inverter output voltages are defined by the following equations:

$$\begin{cases} V_{AN} = \frac{1}{3}.(2.V_{AO} - V_{BO} - V_{CO}) \\ V_{BN} = \frac{1}{3}.(2.V_{BO} - V_{AO} - V_{CO}) \\ V_{CN} = \frac{1}{3}.(2.V_{CO} - V_{BO} - V_{AO}) \end{cases} \quad (34)$$

Considering that the converter is balanced, the floating voltages are well distributed:

$$V_{ci} = \frac{i.U_{bus}}{K} \quad (35)$$

where K is the number of cells per each arm and i indicates the cell concerned.

Thence, the floating voltages of the capacitors become:

$$\begin{cases} V_{cj1} = \frac{U_{bus}}{4} \\ V_{cj2} = \frac{2.U_{bus}}{4} \\ V_{cj3} = \frac{3.U_{bus}}{4} \end{cases} \quad (36)$$

with j (j=A, B, C) denoting the phase.

Accordingly, the inverter output voltages become:

$$\begin{cases} V_{AO} = \frac{U_{dc}}{4}.(S_{A1} + S_{A2} + S_{A3} + S_{A4}) \\ V_{BO} = \frac{U_{dc}}{4}.(S_{B1} + S_{B2} + S_{B3} + S_{B4}) \\ V_{CO} = \frac{U_{dc}}{4}.(S_{C1} + S_{C2} + S_{C3} + S_{C4}) \end{cases} \quad (37)$$

3.2. Filter modeling

This is a low-pass filter comprising an inductor L and a resistor R in series.

In dq-frame, the direct and quadrature components of the modulated voltages to the output of multicellular converter are given by:

$$\begin{cases} V_{Nd} = R.i_d + L.\frac{d}{dt}i_d - L.w_R.i_q + V_{Rd} \\ \quad = V_{Nd1} - L.w_R.i_q + V_{Rd} \\ V_{Nq} = R.i_q + L.\frac{d}{dt}i_q + L.w_R.i_d + V_{Rq} \\ \quad = V_{Nq1} + L.w_R.i_d + V_{Rq} \end{cases} \quad (38)$$

where R and L are respectively the resistance and inductance of the filter, i_d and i_q are direct and quadrature currents of the electric line, V_{Rd} and V_{Rq} are the direct and quadrature

voltages of the grid, V_{Nd} and V_{Nq} are the inverter control voltages, and w_R is the grid frequency.

The filter model in the d-q frame is represented by the following figure:

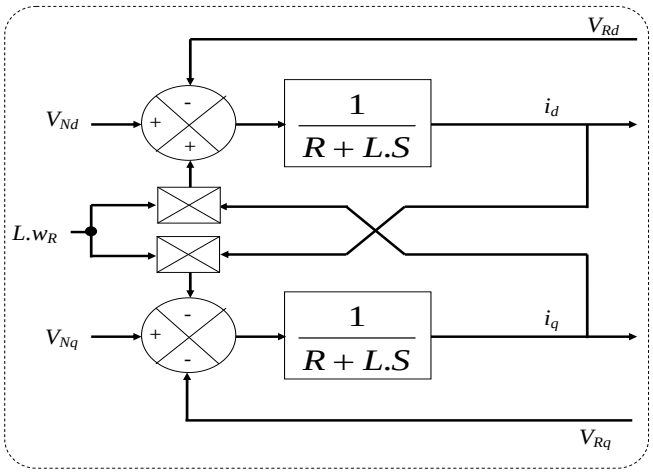

Fig. 7. Filter model

3.3. Inverter control

The studied wind farm is connected to the electrical network characterized by a frequency f=50Hz and a V_R voltage through a multicellular inverter and a filter RL. This converter allows to establishing the current at mains frequency and controlling the reactive and active powers injected into the grid.

The powers transmitted to the grid are defined by:

$$\begin{cases} P_R = V_{Rd}.i_d + V_{Rq}.i_q \\ Q_R = V_{Rq}.i_d - V_{Rd}.i_q \end{cases} \quad (39)$$

It is found that the active power P_R well as reactive power Q_R is based on the direct component and the quadratic component of the current grid. The problem here is to independently control the reactive and active powers. To do this, simply steer (d, q) so as to cancel the component of the quadrature voltage (V_{Rq} = 0), and consequently $V_R = V_{Rd}$. The equation (41) and equation (42) become:

$$\begin{cases} V_{Nd} = R.i_d + L.\dfrac{d}{dt}i_d - L.w_R.i_q + V_{Rd} \\ \quad = V_{Nd1} - L.w_R.i_q + V_R \\ V_{Nq} = R.i_q + L.\dfrac{d}{dt}i_q + L.w_R.i_d \\ \quad = V_{Nq1} + L.w_R.i_d \end{cases} \quad (40)$$

$$\begin{cases} P_R = V_R.i_d \\ Q_R = -V_R.i_q \end{cases} \quad (41)$$

For to operate the system at a unity power factor, we impose a reference reactive power equal to zero ($Q_{R\text{-}ref}$ = 0).

The reactive and active powers provide the currents $i_{d\text{-}ref}$ and $i_{q\text{-}ref}$.

$$\begin{cases} i_{d-ref} = \dfrac{P_{R-ref}.V_{Rd} + Q_{R-ref}.V_{Rq}}{V^2_{Rd} + V^2_{Rq}} = \dfrac{P_{R-ref}\cdot}{V_R} \\ i_{q-ref} = \dfrac{P_{R-ref}.V_{Rq} - Q_{R-ref}.V_{Rd}}{V^2_{Rd} + V^2_{Rq}} = 0 \end{cases} \quad (42)$$

The active power reference injected into the grid is defined by [24]:

$$P_{R-ref} = P_g - P_{bus} \quad (43)$$

where the power stored by the DC bus capacitors P_{bus} and the active power produced by the generators P_g are given by the following equations:

$$\begin{aligned} P_g &= P_{g1} + P_{g2} + P_{g3} \\ &= U_{bus}(I_{m1} + I_{m2} + I_{m3}) \end{aligned} \quad (44)$$

$$P_{bus} = U_{bus}.i_{bus} \quad (45)$$

The block diagram of the control loops of the currents injected into the grid is given by the figure below:

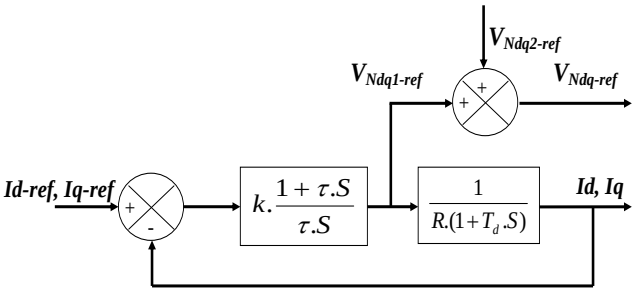

Fig. 8. Control system of grid currents

where $K = 3\dfrac{L}{t_r}$ is the gain of the controller, tr is the response time and $T_d = \tau = 3\dfrac{L}{R}$ is the coefficient of the integral controller.

3.4. Pulse width modulation

We have used the natural pulse width modulation for generating the command signals for each cell of the inverter. These orders are to be out of phase by $\dfrac{2\pi}{K}$ between them. The control signals of each cell are obtained by intersecting the triangular signals defined by equation (49) (tr1, tr2, tr3, tr4) with the modulating signal associated with each cell (VAN*, VBN*, VCN*).

$$\begin{cases} t_{r1} = \frac{\pi}{2}\arcsin(\sin(2.\pi.f_H - \frac{\pi}{2})) \\ t_{r2} = \frac{\pi}{2}\arcsin(\sin(2.\pi.f_H - \pi)) \\ t_{r3} = \frac{\pi}{2}\arcsin(\sin(2.\pi.f_H - \frac{3.\pi}{2})) \\ t_{r4} = \frac{\pi}{2}\arcsin(\sin(2.\pi.f_H - 2.\pi)) \end{cases} \quad (46)$$

Each arm of the inverter contains four cells, so it needs four control signals. For example the simile between the reference signal VAN* and the four triangular signals gives the four control signals applied to the arm A, which is the same for both B and C arms.

The generation strategy of the inverter control commands is represented by the following figure.

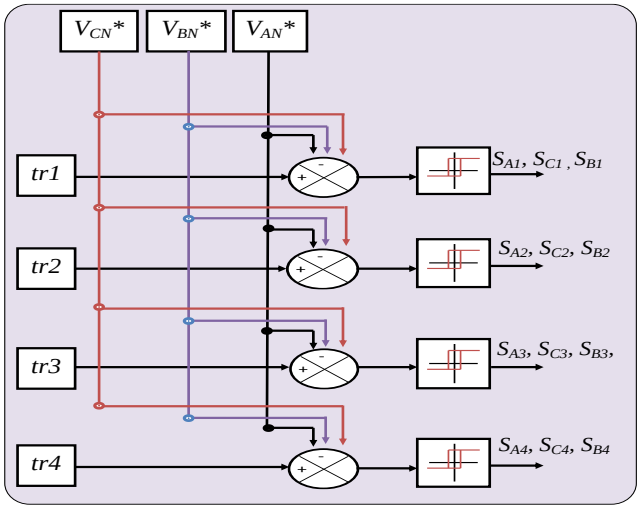

Fig. 9. Generating block of the inverter control signals

The inverter control system is shown in Fig.10:

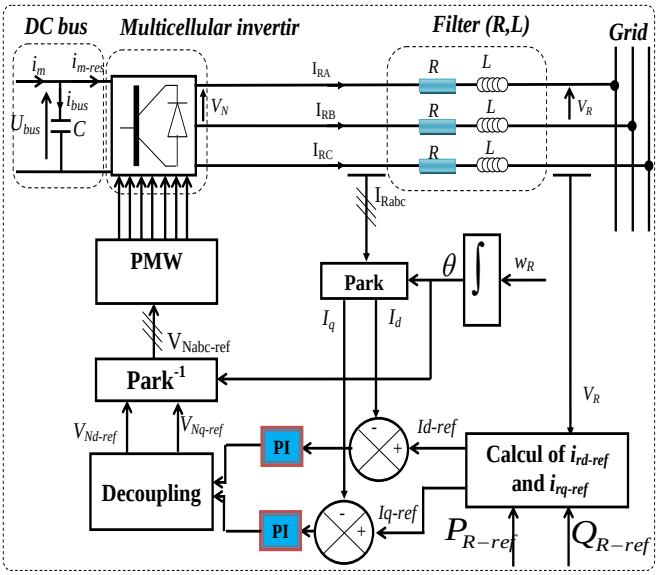

Fig. 10. Control scheme of inverter

4. Simulation Results

The simulation results are obtained using the Matlab/Simulink environment. To confirm the control strategies providing wind energy management, we have applied a wind profile given by Fig.11a over a period of 50s for the three turbines.

To secure the wind turbines against mechanical failures during high wind speed, a system for adjusting the pitch angle of the blades has been established, as indicated in Fig.11b. This mechanism is used to limit wind power during strong wind.

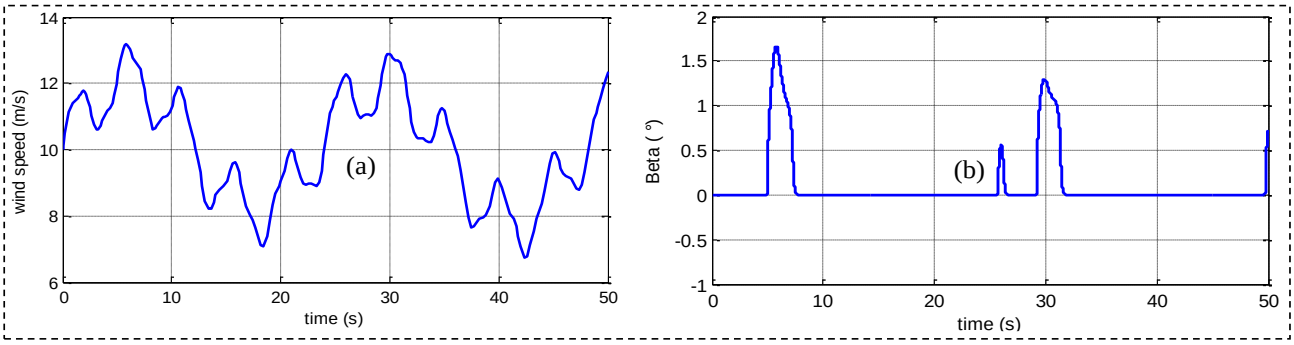

Fig. 11. (a) Wind speed profile, (b) Local control of pitch angle β

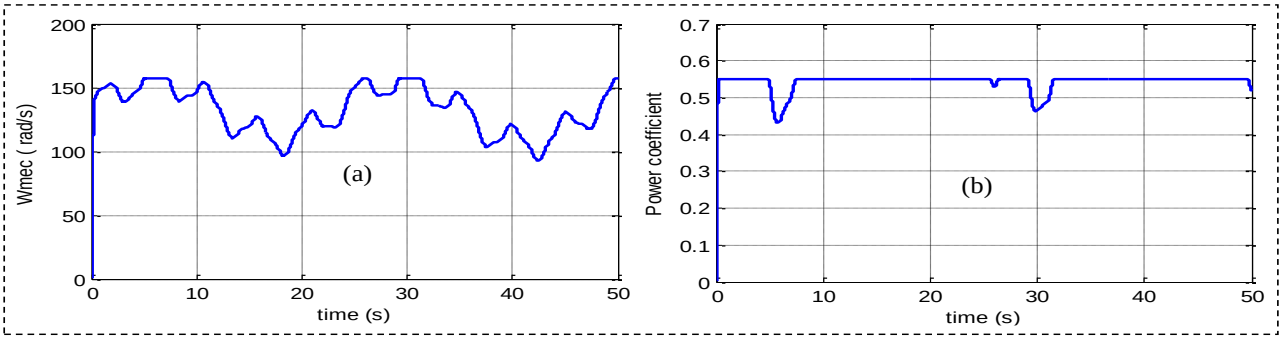

Fig 12. (a) PMSG speed, (b) Power coefficient *Cp*

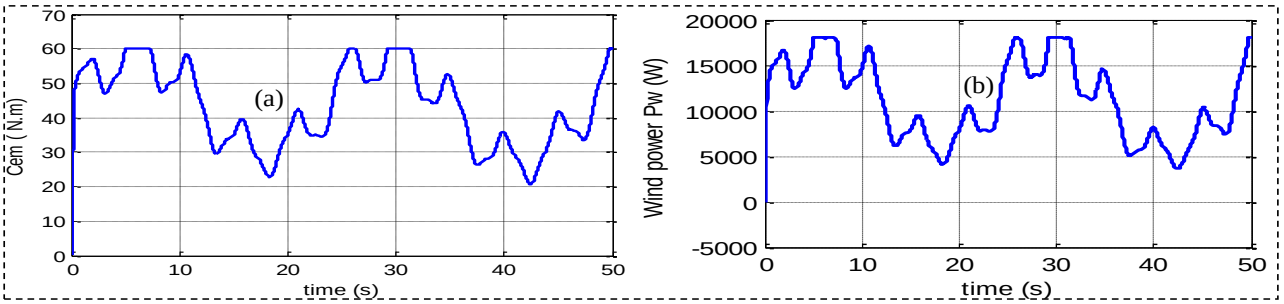

Fig. 13. (a) Electromagnetic torque C_{em}, (b) Wind power Pw

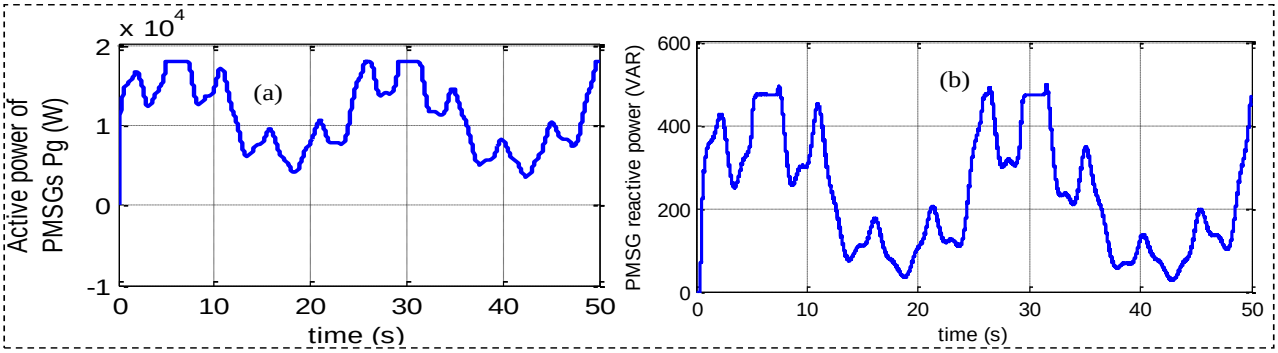

Fig. 14. (a) Simulated active powers P, (b) Simulated reactive powers Q

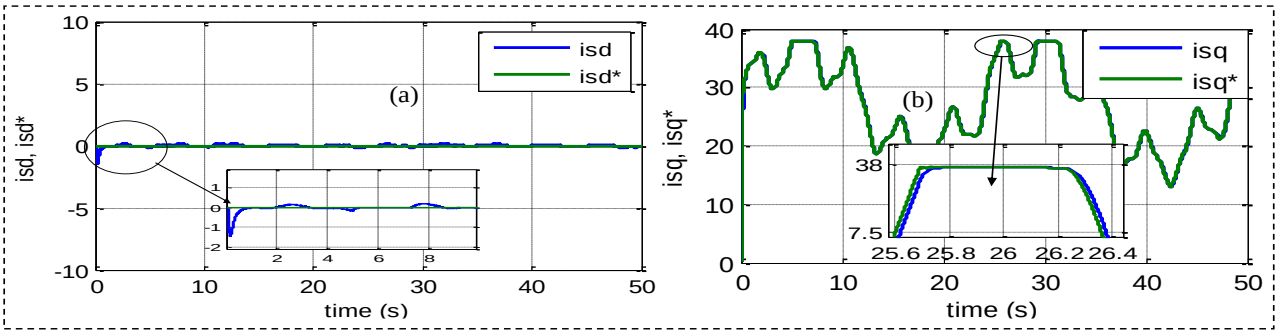

Fig. 15. (a) Direct component of stator currents in dq referential, (b) Quadrature component of stator currents in dq referential

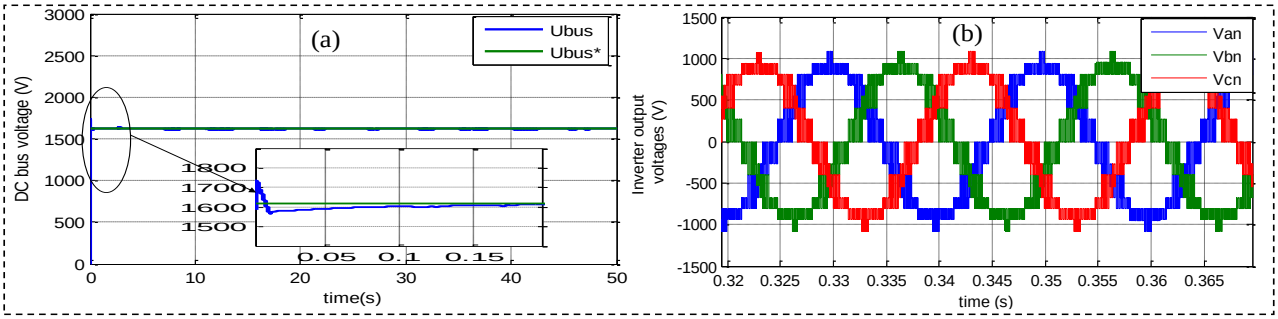

Fig. 16. (a) DC bus voltage $U_{dc,}$ (b) Inverter output voltages.

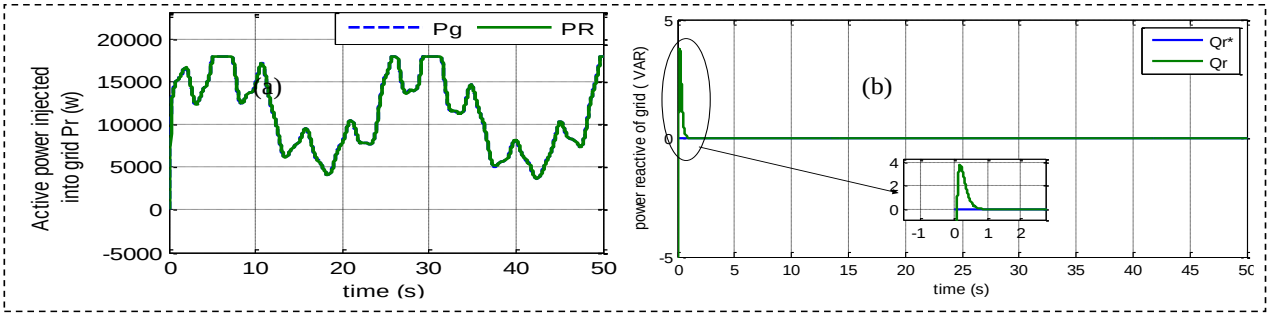

Fig. 17. (a) Active power Pr, (b) Reactive power Qr

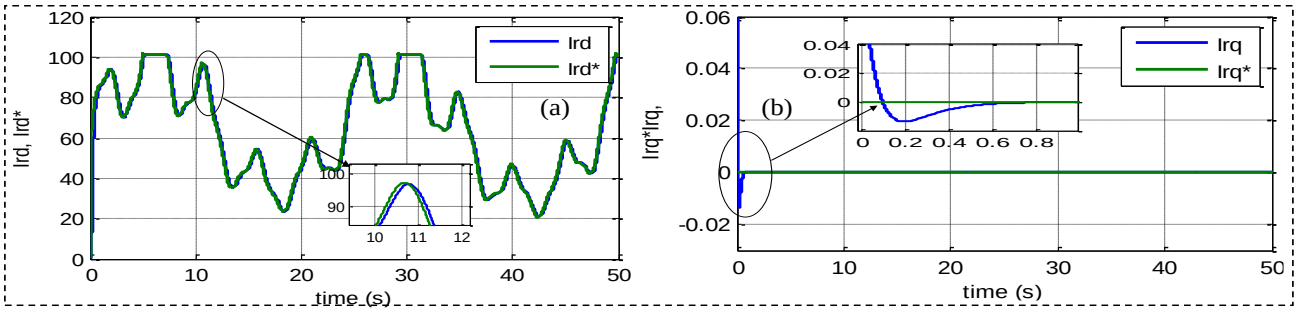

Fig. 18. (a) Direct current i_{rd}, (b) Quadrature current i_{rq}

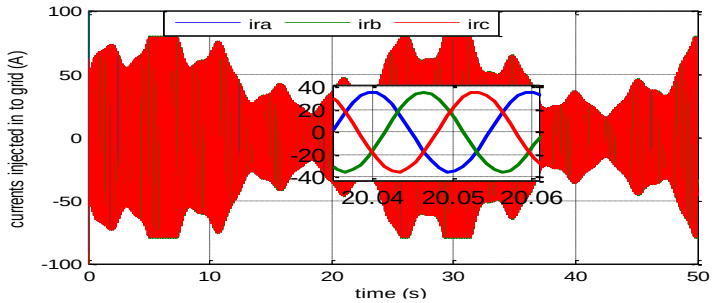

Fig. 19. Grid currents ir_{abc}

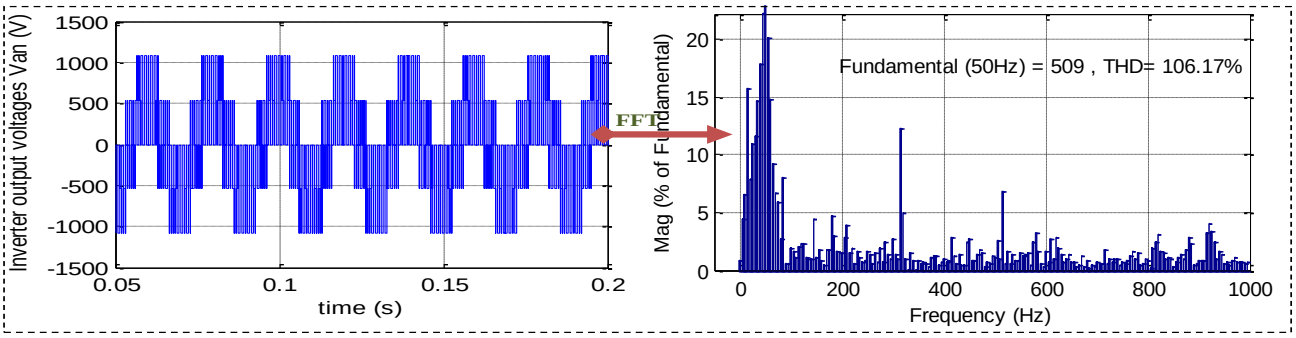

Fig. 20. Harmonic spectrum of output voltage of two levels inverter plotted with FFT analysis of Simulink.

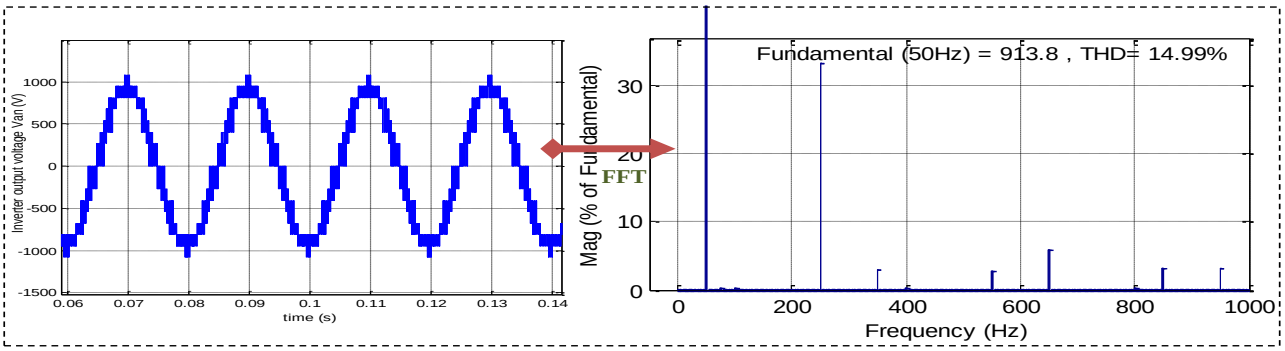

Fig. 21. Harmonic spectrum of output voltage of multicellular inverter plotted with FFT analysis of Simulink.

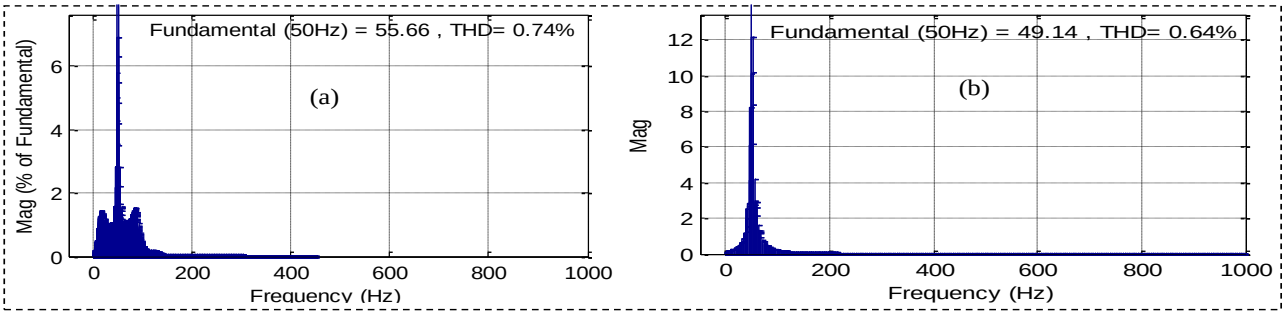

Fig. 22. Harmonic spectrum of output current injected into grid plotted with FFT analysis of Simulink: (a) by using a classical two-level inverter, (b) by using a multicellular inverter

Figure 12a shows the mechanical speed of the machine. This speed is restricted to its nominal speed thanks to a control algorithm of the angle β applied to our farm. The wind farm is controlled in order to capture the maximum of wind power available, so this farm operates under an MPPT control However, when the turbine speed outdated its nominal value, the angle β increases to decrease the coefficient C_P (Fig.12b), which aims to maintain the mechanical speed and the generated power constants.

It is clear to note that the electromagnetic torque given by Fig.13a and the total power produced by the three wind turbines represented by Fig.13b are well correlated with the wind speed.

Figure 14a shows the active power produced by the three generators. Each generation is commanded to produce the rated power in case of high wind speed. Figure 14b illustrates the reactive power produced by the farm.

Figure 15a and Figure 15b respectively show the evolution of stator currents i_{sd} and i_{sq} for the generator 2 with the PI controller. The answers show that the controller provides a good performance.

Figure 16a shows that the DC bus voltage is equal at its reference value 1620 V, thus proving the effectiveness of the implanted controller. The inverter output signals are represented by Fig. 16b. They vary sinusoid-ally at a constant frequency equal to 50 Hz, with a number of very important levels per alternately.

Figure 17b and Figure 17a confirm that the control loops and the reactive and active power supplied to the electricity network have kept to their reference values. The reactive power is zero, proving the functioning with a unity power factor. We can notice after this figure that the balance between generated and consumed power is reached during the operation of the system.

Fig. 18a and Fig. 18b respectively show the evolution of direct and quadrature currents injected into the grid i_{rd} and i_{rq}. The answers show that the controller provides a good performance.

The currents injected into the grid, represented by Fig.19, are sinusoidal at a frequency equal to the grid frequency and take variable amplitudes from to the variations in wind speed.

- Spectral analysis

To evaluate the capabilities of studied wind farm to minimize the harmonics of the currents injected into the grid, the spectra of the modulated voltages by the electrical network side converter are presented in Fig. 20 and Fig. 21. Indeed, Fig.20 shows that the Total Harmonic Distortions (THD) when using a conventional inverter with two levels is 106.17%. On the other hand, Fig.21 shows that this THD is considerably reduced to 14.99%, which demonstrates the performance of flying-capacitor multicellular inverters in industrial applications.

So as to evaluate the harmonic content of the current injected in the grid, the THD is considered using Fast Fourier Transform (FFT) analysis. A comparative study presented in Fig.22 between the THD of the current grid in the case of using a classical two level inverter and in the case of using a multicellular inverter. A comparison between these two topologies of inverters shows that an improvement, in terms of harmonic mitigation, is accomplished by using the multicellular inverter. In fact, the enhancement of the electrical network current THD is 0.64% for the multicellular inverter and 0.74% for the classical inverter.

Table 1. Studied wind turbine parameters.

Wind turbine	Number of blades	3
	ρ	1.225 Kg/m3
	R	2
PMSG	Rs	0.82 Ω
	Ls	15.1 mH
	p	4
	$Flux\ \Phi_m$	0.4832 Wb
DC bus	C_{bus}	2200µF
	$U_{bus\text{-}ref}$	1620V
Grid-side filter	R	0.2 Ω
	L	25 mH

5. Conclusion

In this article, a new control strategy for a wind farm with three aero-generators has been developed. This technique is treated to remove the instability from production without adding any storage organs to guarantee the equivalence between consumption and production, so as to command the DC bus voltage and the power exchange between the farm and the electrical network. This document has also studied the prolonged use of a multicellular inverter with four cells in order to improve the quality of the voltage modulated by the converter. The simulation results, obtained by Matlab/Simulink, validate the developed control strategies.

References

[1] Glasnovic Z, Margeta J. "Vision of total renewable electricity scenario", Renew Sust Energy Rev vol. 15, n°. 4, pp.1873–1884, 2011.

[2] Chowdhury SP, Chowdhury S, Crossley PA. UK. "Scenario of islanded operation of Active distribution networks with renewable distributed generators". International Journal of Electrical Power & Energy Systems, vol. 33, n°. 7, pp. 1251–1255, 2011.

[3] Sanseverino ER, Di Silvestre ML, Ippolito MG, De Paola A, Re GL. "An execution, monitoring and replanting approach for optimal energy management in micro-grids". Energy, vol. 36, n°. 5, pp. 3429–3436, 2011.

[4] N. Pogaku, M. Prodanovic, T. Green, "Modeling, Analysis and Testing of Autonomous Operation of an Inverter- Based Micro-grid," *IEEE Trans. Power Electron*, vol. 22, pp. 613-625, 2007.

[5] A.A. Bhuiyan, A.K.M.S. Islam, A.I. Alam, "Application of Wind Resource Assessment (WEA) tool: A case study in Kuakata, Bangladesh," International Journal of Renewable Energy Research, vol. 1, pp. 83-90, 2011.

[6] Wen J, Zheng Y, Donghan F, "A review on reliability assessment for wind power", Renew Sustain Energy Rev, vol. 13, n°. 9, pp. 2485–2494, 2009.

[7] Hoogwijk M, De Vries B, Turkenburg W, "Assessment of the global and regional geographical, technical and economic potential of onshore wind energy", Energy Econom, vol. 26, n°. 5, pp. 889–919, 2004.

[8] Lund H, Clark WW, "Management of fluctuations in wind power and CHP comparing two possible Danish strategies", Energy, vol. 27, n°. 5, pp. 471-483, 2002.

[9] Rabiee, A., Khorramdel, H., Aghaei, J, "A review of energy storage systems in micro-grids with wind turbines", Renewable and Sustainable Energy Reviews, vol. 18, pp. 316-326, 2013.

[10] Abbey C, Joos G, "Super-capacitor energy storage for wind energy applications", IEEE Trans Ind Appl, vol. 43, n°. 3, pp. 769-776, 2007.

[11] McDowall J, "Integrating energy storage with wind power in weak electricity grids", J Power Sources, vol. 162, n°. 2, pp. 959-964, 2006.

[12] Donald Grahame Holmes, Brendan P. McGrath, "Opportunities for Harmonic Cancellation with Carrier-Based PWM for Two-Level and Multilevel Cascaded Inverters", IEEE transactions on industry applications, vol. 37, n°. 2, pp. 574-582, march-April 2001.

[13] T.Meynard, H. Foch, P. Thomas, J. Courault, R. Jacob, andM. Nahrstaedt, "Multicell converters: Basic concepts and industry applications," IEEE Trans. Ind. Electron., vol. 49, nº. 5, pp. 955–964, Oct 2002.

[14] D. Krug, M. Malinowski, and S. Bernet, "Design and comparison of medium voltage multi-level converters for industry applications", 39th IEEE IAS Annual Meeting, in Conference Record. vol. 2, pp. 781–790, 2004.

[15] T. Meynard, M. Fadel, and N. Aouda, "Modeling of multilevel converters," *IEEE Trans. Ind. Electron.*, vol. 44, n°. 3, pp. 356–364, Jun 1997.

[16] Masmoudi A, Abdelkafi A, Krichen L. "Electric power generation based on variable speed wind turbine under load disturbance". Energy, vol. 36, n°. 8, pp. 5016–5026, 2011.

[17] Minh Quan Duong, Francesco Grimaccia, Sonia Leva, Marco Mussetta, Emanuele Ogliari, "Pitch Angle Control Using Hybrid Controller for All Operating Regions of SCIG Wind Turbine System", Renewable Energy, vol. 70, pp. 197- 203, 2014.

[18] Muhando EB, Senjyua T, Urasakia N, Yonaa A, Kinjob H, Funabashi T, "Gain scheduling control of variable speed WTG under widely varying turbulence loading", Renew Energy, vol. 32, n°. 14, pp. 2407-2423, 2007.

[19] Galdi V, Piccolo A, Siano P, "Exploiting maximum energy from variable speed wind power generation systems by using an adaptive Takagi-Sugeno-Kang fuzzy model", Energy Convers Manage, vol. 50, n°. 2, pp. 413-421, 2009.

[20] R. Chedid, F. Mirad et M. Basma, "Intelligent control of a class of wind energy conversion systems", IEEE Transactions on Energy Conversion, vol. 14, n°. 4, pp.1597-1604, 1999.

[21] J. L. Rodriguez – Amenedo, S. Arnalte et J. C. Burgos, " Automatic generation control of wind farm with variable speed wind turbine ", IEEE Transactions on Energy Conversion, vol. 17, n°. 2, pp. 279-284, 2002.

[22] Mouna Rekik, Achraf Abdelkafi, Lotfi Krichen, "A novel control strategy of a distributed generator operating in seven modes for ancillary services under grid faults", International Journal of Electrical Power and Energy Systems, vol. 47, pp. 100-108, 2013.

[23] François Defaÿ, Ana-Maria Llor, Maurice Fadel, "A Predictive Control With Flying Capacitor Balancing of a Multicell Active Power Filter", IEEE transactions on industrial electronics, vol. 55, n°. 9, pp. 3212-3220, september 2008.

[24] M.Mansour, M.N.Mansouri, M.F.Mmimouni, "Study and Control of a Variable-Speed Wind-Energy System Connected to the Grid" international journal of renewable energy research, vol. 1, no. 2, pp. 96-104 , 2011.